NUMISHEET 2022

Proceedings of the 12th International Conference and Workshop on Numerical Simulation of 3D Sheet Metal Forming Processes

EDITED BY
Kaan Inal
Julie Levesque
Michael Worswick
Cliff Butcher

TMS

Springer

The Minerals, Metals & Materials Series

Kaan Inal · Julie Levesque · Michael Worswick · Cliff Butcher
Editors

NUMISHEET 2022

Proceedings of the 12th International Conference and Workshop on Numerical Simulation of 3D Sheet Metal Forming Processes

TMS

Springer

Editors
Kaan Inal
University of Waterloo
Waterloo, ON, Canada

Julie Levesque
Quebec Metallurgy Center
Montreal, QC, Canada

Michael Worswick
University of Waterloo
Waterloo, ON, Canada

Cliff Butcher
University of Waterloo
Waterloo, ON, Canada

ISSN 2367-1181 ISSN 2367-1696 (electronic)
The Minerals, Metals & Materials Series
ISBN 978-3-031-06211-7 ISBN 978-3-031-06212-4 (eBook)
https://doi.org/10.1007/978-3-031-06212-4

This Springer imprint is published by the registered company Springer Nature Switzerland AG
The registered company address is: Gewerbestrasse 11, 6330 Cham, Switzerland

Contents

Part VII Modelling of Failure

Part VIII Modelling of Friction

Part I
Numerical Implementation of Advanced Constitutive Models

A New Trial Stress for Newton's Iteration Based on Plastic Strain Rate Potential

Seung-Yong Yang and Wei Tong

Abstract It is known that Newton's iteration can be divergent for highly anisotropic yield functions with a large strain increment in finite element analysis of plastic deformation. One of the reasons of the divergence is inaccurate estimation of the initial stress by elastic trial stress. The line search strategy cannot completely remove the problem. A new method to predict the trial stress by plastic strain rate potential was proposed in this work. The new method was applied to Hill's quadratic yield function and Hershey-Hosford yield function. It was shown that the number of iterations can be reduced significantly for plane stress biaxial loading, and computation time can be saved for 3-dimensional finite element simulation.

Keywords Newton iteration · Plasticity potentials · Trial stress

Introduction

Finite element analysis of plastic deformation requires constitutive update of the stress and plastic strain of the material along the loading path, and the new state of the structure will be found by solving a system of equations for the nodal displacements in the main program. The constitutive equations of plastic materials are nonlinear, and a numerical solution of the equations for the stress and plastic strain needs an iterative process in the material routine. Newton's method is widely used for the iterative solution procedure.

If the material exhibits highly anisotropic behavior in the plastic deformation and the load increment is large, Newton's iteration can diverge and more sophisticated methods are necessary to obtain a converged solution. It was reported that Newton's iteration can be divergent for a highly anisotropic yield function or a higher value of

S.-Y. Yang (✉)
Korea University of Technology and Education, Chungnam 31253, Korea
e-mail: ysy@koreatech.ac.kr

W. Tong
Southern Methodist University, Dallas, TX 75275, USA
e-mail: wtong@smu.edu

K. Inal et al. (eds.), *NUMISHEET 2022*, The Minerals, Metals & Materials Series,
https://doi.org/10.1007/978-3-031-06212-4_1

the exponent in the Hershey-Hosford yield when a large strain increment is imposed [1]. Line search method was proposed to resolve this issue and enhance the convergence property of the Newton method [1, 2]. In these methods, they assumed an elastic trial stress with vanishing plastic strain increment, and then the line search method was applied to choose an appropriate plastic strain increment to reduce error in the iteration. However, the line search method cannot provide a complete solution to the problem, and the iteration still can be divergent. One of the main reasons for the problem seems that the elastic trial stress is overwhelmingly large when the strain increment is large. Manik [3] proposed a radial return method to improve the convergence of Newton iteration and saved computation time for Hill's quadratic and Yld2004-18p yield functions.

In this paper, a plastic trial stress was proposed to replace the conventional elastic trial stress for the Newton iteration. The new trial stress is based on dual plastic strain rate potential which is a function of plastic strain rate and dual to the yield function. If a plastic strain rate is assumed approximately, then a stress state on the yield surface can be obtain by using the orthogonality condition to the dual plastic strain rate potential and the stress will be closer to the actual stress than the elastic prediction. This yield stress was used as the initial trial stress for the Newton iteration. The effectiveness of the new plastic trial stress in the iterative procedure and finite element analysis was presented in comparison to the conventional elastic trial stress. A review of Newton's method and the proposal of the plastic trial stress will be presented in the framework of the associated flow rule in next sections, and the plastic strain rate potentials for Hill's quadratic yield function and Hershey-Hosford yield function will be described in the following section. The proposed algorithm was implemented in ABAQUS user material subroutine (UMAT) and its numerical superiority will be displayed in comparison for simple biaxial loadings and a general 3-D loading.

Newton's Method and Plastic Trial Stress

Newton Iteration

Stress-based yield potentials are useful in elasto-plastic deformation analyses. Newton's iteration based on the yield function $f(\boldsymbol{\sigma})$ will be described in this section. That is, the yield condition will be applied and the plastic strain increment should satisfy the normality rule to the yield surface. Suppose we are given a stress and equivalent plastic strain at the current time t and a strain increment $\Delta\boldsymbol{\epsilon}$ for the next time $t + \Delta t$. If the corresponding yield function to the elastic trial stress is large enough to satisfy the current yield condition, the material will undergo plastic deformation. Then the new yield condition and the normality rule should be satisfied at the new time $t + \Delta t$, i.e.,

$$r = f(\boldsymbol{\sigma}(t) + \Delta\boldsymbol{\sigma})) - \sigma_f(\bar{\epsilon}^p(t) + \Delta\bar{\epsilon}^p) = 0 \tag{1}$$

$$\mathbf{R} = \left(\Delta\boldsymbol{\epsilon} - \mathbf{C}^{-1}\Delta\boldsymbol{\sigma}\right) - \Delta\bar{\epsilon}^p \frac{\partial f}{\partial \boldsymbol{\sigma}}(\boldsymbol{\sigma}(t) + \Delta\boldsymbol{\sigma}) = \mathbf{0} \tag{2}$$

where $\Delta\bar{\epsilon}^p$ is the increment of the equivalent plastic strain during Δt. The small deformation assumption was used, so that the total strain increment is the sum of the elastic and plastic parts in Eq. (2). The flow potential is the same as the yield function in the associated plasticity. The solution of the above two equations are $\Delta\bar{\epsilon}^p$ and $\Delta\boldsymbol{\sigma}$. If a trial value is assumed for $\Delta\bar{\epsilon}^p$ in Eq. (2) and the Taylor expansion is considered, then Eq. (2) will give $\Delta\boldsymbol{\sigma}$. These trial $\Delta\bar{\epsilon}^p$ and $\Delta\boldsymbol{\sigma}$ are substituted in Eq. (1) to check whether the equation is satisfied. If not, some modification on the assumed $\Delta\bar{\epsilon}^p$ is made until the yield condition is satisfied. This procedure can be formulated in the framework of Newton's method to give a systematic modification on the increments of the equivalent plastic strain and stress. That is, the following variations can be derived.

$$\delta\Delta\bar{\epsilon}^p = \frac{r + \mathbf{n} : \mathbf{L}\mathbf{R}}{\mathbf{n} : \mathbf{L}\mathbf{n} + h} \tag{3}$$

$$\delta\Delta\boldsymbol{\sigma} = \mathbf{L}\left(\mathbf{R} - \delta\Delta\bar{\epsilon}^p\mathbf{n}\right) \tag{4}$$

where r and $\mathbf{R}$ are the current residuals and $\mathbf{n}$, $\mathbf{L}$ and h are defined in Eqs. (5)–(7). Modified new increments are to be given by the sum of the old increments and the variations of (3) and (4).

$$\Delta\bar{\epsilon}^{p\,(new)} = \Delta\bar{\epsilon}^{p\,(old)} + \delta\Delta\bar{\epsilon}^p$$
$$\Delta\boldsymbol{\sigma}^{(new)} = \Delta\boldsymbol{\sigma}^{(old)} + \delta\Delta\boldsymbol{\sigma}.$$

Newton's iteration will continue until these $\Delta\bar{\epsilon}^{p\,(new)}$ and $\Delta\boldsymbol{\sigma}^{(new)}$ satisfy Eqs. (1) and (2) with enough accuracy (that it, the residuals r and $\mathbf{R}$ are small enough). The following variables need to be updated during the iteration.

$$\mathbf{n} = \frac{\partial}{\partial\boldsymbol{\sigma}} f\left(\boldsymbol{\sigma}(t) + \Delta\boldsymbol{\sigma}\right) \tag{5}$$

$$h = \frac{\partial}{\partial\Delta\bar{\epsilon}^p}\sigma_f(\bar{\epsilon}^p + \Delta\bar{\epsilon}^p) \tag{6}$$

$$\mathbf{L} = \left(\mathbf{C}^{-1} + \Delta\bar{\epsilon}^p \frac{\partial^2}{\partial\boldsymbol{\sigma}^2} f(\boldsymbol{\sigma}(t) + \Delta\boldsymbol{\sigma})\right)^{-1} \tag{7}$$

To initiate Newton's iteration described above, $\Delta\bar{\epsilon}^p$ and $\Delta\boldsymbol{\sigma}$ need to be assumed first. The number of iterations will depend on how much accurately the initial guesses were made close to the true solution. This entails the concept of the plastic trial stress described in the next section.

Plastic Trial Stress

In conventional numerical procedure for plasticity, the elastic trial stress is assumed by $\Delta\boldsymbol{\sigma} = \mathbf{C}\Delta\boldsymbol{\epsilon}$ and vanishing plastic strain increment ($\Delta\bar{\epsilon}^p = 0$) is used as the initial value for Newton's iteration. These trial values seem straightforward, but they can be inaccurate if the strain increment is large, and many iterations can be caused or the iteration can be divergent for highly anisotropic materials. To obtain better trial increments, plastic stress which is based on the plastic strain rate potential will be considered as the new trial stress in place of the elastic trial stress.

Yield stress state can be given by the orthogonality condition to the plastic strain rate in the theory of dual plastic potentials [4].

$$\boldsymbol{\sigma}(t + \Delta t) = \nu \frac{\partial}{\partial \Delta\boldsymbol{\epsilon}^p} q(\Delta\boldsymbol{\epsilon}^p) \tag{8}$$

where the parameter ν is equal to the yield strength along the rolling direction, $\nu = \sigma_f(\bar{\epsilon}^p(t) + \Delta\bar{\epsilon}^p)$ in the associated plasticity. There can be many possible options for the plastic strain increment $\Delta\boldsymbol{\epsilon}^p$ and $\Delta\bar{\epsilon}^p$. One simple way is to assume $\Delta\boldsymbol{\epsilon}^p = \Delta\boldsymbol{\epsilon}$ and $\Delta\bar{\epsilon}^p = q(\Delta\boldsymbol{\epsilon}^p)$. These assumptions can define a plastic trial stress by Eq.(8). Another more sophisticated approach is to take only a fraction of the full strain increment for the plastic strain increment in reference to Manik's paper [3]. He proposed a radial projection of the elastically predicted stress $\boldsymbol{\sigma}^{tr}$ on the current yield surface as

$$f\left((1 - \alpha_y)\boldsymbol{\sigma}^{tr}\right) = \sigma_f(\bar{\epsilon}^p(t))$$

where $\alpha_y \in [0, 1]$ is the solution of the above equation. Then $(1 - \alpha_y)\boldsymbol{\epsilon}$ will be the corresponding total elastic strain, and the remaining $\alpha_y\boldsymbol{\epsilon}$ will be the plastic strain increment. Hence $\Delta\boldsymbol{\epsilon}^p = \alpha_y\boldsymbol{\epsilon}$ was chosen as the trial plastic strain increment to define the equivalent plastic strain increment and equivalent stress as follows

$$\begin{aligned} \Delta\bar{\epsilon}^p &= q\left(\alpha_y\boldsymbol{\epsilon}\right) \\ \bar{\sigma} &= \sigma_f(\bar{\epsilon}^p(t) + \Delta\bar{\epsilon}^p) \end{aligned}$$

These equations will be combined with Eq. (8) to give the plastic trial stress. Then $\Delta\bar{\epsilon}^p$ and $\boldsymbol{\sigma}(t + \Delta t)$ will be used as the initial guess of the plastic strain increment and stress, and Newton's iteration will continue until an accurate enough numerical solution is obtained. The error of the iteration is defined based on the scalar and tensor residuals r and $\mathbf{R}$ as

$$E = \left(\frac{r}{2\mu}\right)^2 + \mathbf{R} : \mathbf{R} \tag{9}$$

where μ is the shear modulus. If the error is small enough during the iteration, for example $E < 10^{-10}$, then the approximate solution was regarded as being close enough to the true solution, and the iteration is terminated.

Yield Functions and Their Plastic Strain Rate Potentials

Hill's Quadratic Yield Function

Hill's quadratic yield function $f(\boldsymbol{\sigma})$ is defined by [5]

$$\begin{aligned} 2f^2(\boldsymbol{\sigma}) &= F(\sigma_{yy}-\sigma_{zz})^2 + G(\sigma_{zz}-\sigma_{xx})^2 + H(\sigma_{xx}-\sigma_{yy})^2 \\ &\quad +2L\tau_{yz}^2 + 2M\tau_{zx}^2 + 2N\tau_{xy}^2 \\ &= 2A_1(\sigma_{xx}-\sigma_{zz})^2 + 2A_2(\sigma_{xx}-\sigma_{zz})(\sigma_{yy}-\sigma_{zz}) \\ &\quad +2A_3(\sigma_{yy}-\sigma_{zz})^2 + 2A_4\tau_{xy}^2 + 2A_5\tau_{yz}^2 + 2A_6\tau_{zx}^2 \end{aligned} \tag{10}$$

where the following identities hold.

$$\begin{aligned} &2A_1 = G+H, \quad 2A_2 = -2H, \quad 2A_3 = F+H, \\ &A_4 = N, \quad A_5 = L, \quad A_6 = M \end{aligned}$$

The dual plastic strain rate function is assumed in the similar form as

$$q^2(\dot{\boldsymbol{\epsilon}}^p) = B_1(\dot{\epsilon}_x^p)^2 + B_2\dot{\epsilon}_x^p\dot{\epsilon}_y^p + B_3(\dot{\epsilon}_y^p)^2 + B_4(\dot{\gamma}_{xy}^p)^2 + B_5(\dot{\gamma}_{yz}^p)^2 + B_6(\dot{\gamma}_{zx}^p)^2 \tag{11}$$

Under these assumptions, relations between the yield function and the dual plastic strain rate potential can be derived analytically. That it, one can use the property that the plastic strain rates should have the same value of the equivalent plastic strain rate, $q(\dot{\boldsymbol{\epsilon}}^p(\boldsymbol{\sigma})) = \dot{\bar{\epsilon}}^p$, whereas the stresses are on a given yield surface. The following relations should hold between A_i and B_i.

$$\begin{aligned} &B_1 = \frac{4A_3}{4A_1A_3 - A_2^2}, \quad B_2 = -\frac{4A_2}{4A_1A_3 - A_2^2} \\ &B_3 = \frac{4A_1}{4A_1A_3 - A_2^2}, \quad B_4 = \frac{1}{A_4}, \quad B_5 = \frac{1}{A_5}, \quad B_6 = \frac{1}{A_6} \end{aligned}$$

Hershey-Hosford Yield Function

Hershey-Hosford yield function is a non-quadratic isotropic yield function. It generalizes von Mises yield function and approaches to Tresca model as the exponent

increases. Hence the flow direction can vary rapidly at the corners of the yield locus for a big exponent a.

$$f^a(\boldsymbol{\sigma}) = \frac{|\sigma_1 - \sigma_2|^a + |\sigma_2 - \sigma_3|^a + |\sigma_3 - \sigma_1|^a}{2} \tag{12}$$

where σ_i are the principal stresses. For the exact dual potential cannot be derived analytically, the following approximate dual plastic strain rate potential was assumed.

$$q^b(\dot{\boldsymbol{\epsilon}}^p) = \frac{|\dot{\epsilon}_1^p|^b + |\dot{\epsilon}_2^p|^b + |\dot{\epsilon}_3^p|^b}{1 + 2^{1-b}} = \frac{|\dot{\epsilon}_1^p|^b + |\dot{\epsilon}_2^p|^b + |\dot{\epsilon}_1^p + \dot{\epsilon}_2^p|^b}{1 + 2^{1-b}} \tag{13}$$

The value of b can be obtained by the least square method to minimize the deviation from a set of discrete plastic strain rates computed from the yield function [6]. For example, one can obtain b =1.51523 for $a = 6$, and $b = 1.34194$ for $a = 8$.

Numerical Results

To test the convergence behavior of Newton's method, Hill's quadratic yield function and Hershey-Hosford yield function were considered. In this section, we will make use of numerical tests similar to Scherzinger's in [1] to show the superiority of the proposed plastic trial stress for the convergence of Newton's iteration.

The material parameters of Hill's quadratic yield function were given as

$$A_1 = 1.0, \quad A_2 = -1.0513, \quad A_3 = 1.0908,$$
$$A_4 = A_5 = A_6 = 2.9926.$$

The quadratic yield function in Eq. (10) with these parameters characterizes AA6111-T4 sheet metal [7]. The exponent $a = 8$ was used for the Hershey-Hosford yield function in Eq. (12). The Swift power law was used for the hardening as

$$\sigma_f(\bar{\epsilon}^p) = 462.79\left(0.007961 + \bar{\epsilon}^p\right)^{0.2} \quad \text{MPa}$$

Young's modulus is 69 GPa and Poisson's ratio is 0.3.

First, the on-axis plane stress biaxial loading condition was considered to find how many iterations are needed to achieve convergence for the elastic trial stress and plastic trial stress, respectively. The stress state and the plastic strain were assumed zero at time $t = 0$, and a large enough strain increment was applied during time step Δt so that the yield condition is satisfied and the plastic deformation occurs. Procedures in reference [8] was used to impose the plane stress condition on the material technically. The applied plane stress condition can be represented as a point on the biaxial stress plane when the shear stress vanishes. 3200 trial cases which are beyond the initial yield locus and less than 40 times the initial yield stress σ_0 along the

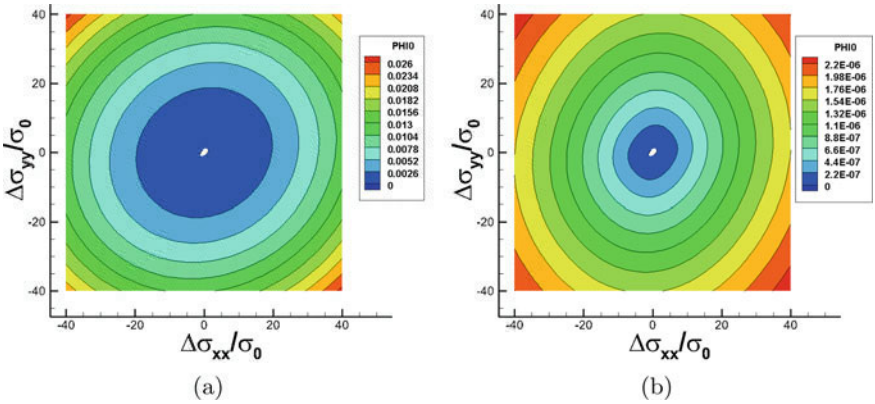

Fig. 1 Error in Eq. (9) by the trial state in the case of **a** elastic trial stress, and **b** plastic trial stress. (Hill's YLD)

rolling direction were examined to test the convergence behavior. The initial residual error in Eq. (9) caused by the trial state before the initiation of the Newton iteration was plotted in Fig. 1a, b for the elastic and plastic trial stresses, respectively, and the number of iterations was plotted for the corresponding trial stresses as shown in Fig. 2. The horizontal axis is the elastic trial stress increment $\Delta\sigma_{xx}$ normalized by the initial yield stress σ_0, and the vertical axis is $\Delta\sigma_{yy}$ normalized by σ_0. The normalized elastic stresses were used to represent the strain increments. The initial error is quite large for the elastic trial stress compared to that of the plastic trial stress as shown in Fig. 1. The number of iterations increased as the elastic trial stress is used even though the line search method was used. Meanwhile, the iteration converged in 1 or 2 iterations without the line search strategy, if the plastic trial stress was used as presented in Fig. 2b. Similar behavior was observed for the Hershey-Hosford model as shown in Figs. 3 and 4. If the elastic trial stress was used then the initial error was huge and the iteration diverged for large loading increments as shown in Fig. 4a (if the number of iterations is greater than 20, then the iteration was regarded as being divergent) although the line search method was applied. Newton's iteration with the plastic trial stress converged very quickly as exhibited in Fig. 4b. These results prove the excellent convergence property of the plastic trial stress.

While it has been shown that the plastic trial stress requires much less iterations for the convergence in the on-axis plane stress biaxial loading, it is necessary to examine if the plastic trial stress actually can reduce the computation time in finite element simulation. ABAQUS/Standard FEA analysis was utilized to compare the computation times for a tensile specimen shown in Fig. 5 which was used by Manik [3]. The specimen has notches and some thickness, so that more general stress conditions can be imposed on the material points. Tensile displacement boundary condition was applied at the end of the specimen along the rolling direction. The constitutive equations were implemented in ABAQUS UMAT subroutine. It is known that the time increment should be reduced to achieve a converged solution in FEA, if the mate-

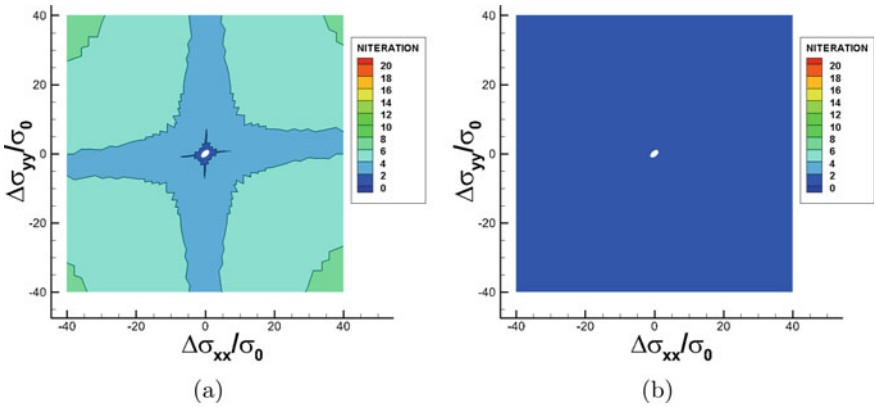

Fig. 2 The number of iterations for the convergence in the case of **a** elastic trial stress, and **b** plastic trial stress. (Hill's YLD)

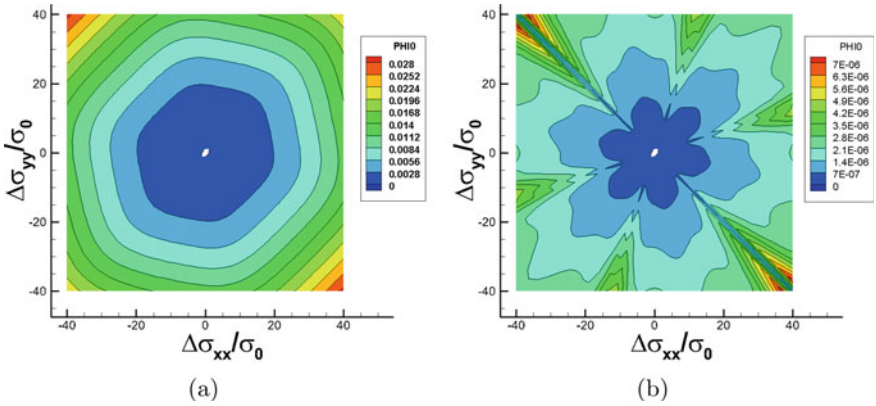

Fig. 3 Error in Eq. (9) by the trial state in the case of **a** elastic trial stress, and **b** plastic trial stress. (Hershey-Hosford YLD with $a = 8$ and $b = 1.34194$)

rial's behavior deviates significantly from the isotropic von Mises plasticity. There are two-time increment options in ABAQUS/Standard, i.e., fixed and automatic. If the time increment is small enough, then the computations have converged for both elastic trial stress and plastic trial stress and the computation times were almost the same. But the time increment is large, then the time increment was automatically controlled and reduced to obtain a converged solution by the ABAQUS main solver. It was observed that the elastic trial stress required a smaller time step for convergence, and more computation time was spent to complete the job as shown in Table 1 for Hill's yield function. The total tensile strain was about 0.06 in the gage section of the specimen. The typical strain increment in the gage section was about 0.0001 for the elastic trial stress, which is smaller than 0.00018 for the plastic trial stress. These strain increments turned out to be much smaller than strain increments for conver-

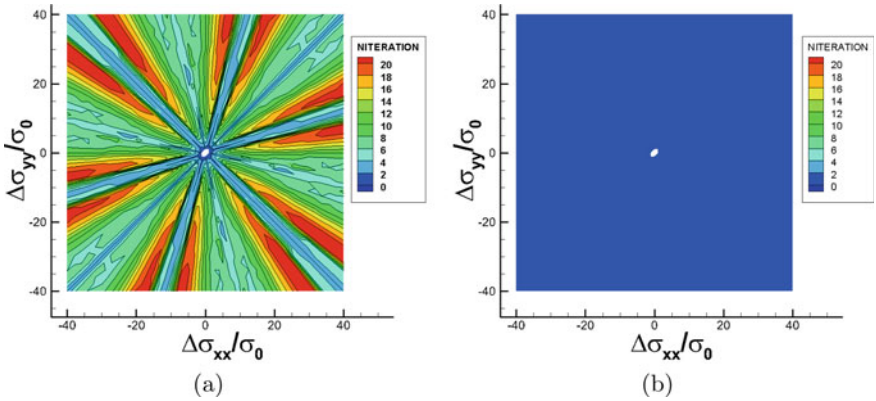

Fig. 4 The number of iterations for the convergence in the case of **a** elastic trial stress, and **b** plastic trial stress. (Hershey-Hosford YLD with $a = 8$ and $b = 1.34194$)

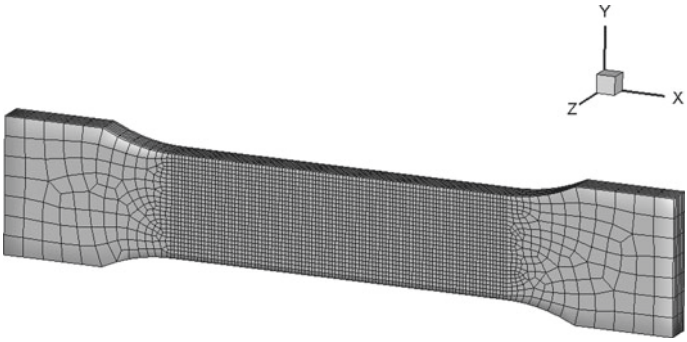

Fig. 5 Tensile specimen [3]

gence in the simple on-axis biaxial loading conditions $\Delta\sigma/\mu$ shown in Figs. 2 and 4. Complicated loading condition in the 3-dimensional specimen seems to restrict the strain increment to the smaller values. ABAQUS intrinsic material library provides Hill's quadratic anisotropic yield function, and the total computation time was more or less similar to the time used in the case of the plastic trial stress, which is significantly less than the time of the elastic trial stress. The line search method was not implemented for the case of the plastic trial stress. If the convergence norm is reduced, then the elastic trial stress and the plastic trial stress required a similar time increment and the total computation times were about the same. ABAQUS does not provide Hershey-Hosford material model, so comparison was made only between the elastic and plastic trial stresses in terms of UMAT as shown in Table 2. The strain increment was about 6×10^{-5} for the elastic trial stress, and the strain increment was 1.4×10^{-4} for the plastic trial stress. Computation time was saved significantly by the usage of the plastic trial stress in Hershey-Hosford model as well.

Table 1 Comparison of computation times of ABAQUS Hill's model and UMATs

Hill	CPU time (s)
ABAQUS Intrinsic material	291.9
Elastic trial stress (UMAT)	652.0
Plastic trial stress (UMAT)	285.0

Table 2 Comparison of computation times of Hershey-Hosford model by UMATs

H-H	CPU time (s)
Elastic trial stress (UMAT)	1508.1
Plastic trial stress (UMAT)	487.8

Discussion and Conclusions

The concept of plastic trial stress was applied to develop an efficient trial stress in Newton's iteration. Hill's quadratic yield and Hershey-Hosford yield were considered for the application and evaluation of the new trial stress. As can be shown by the residual error in biaxial plane stress loading, the plastic trial stress was closer to the true solution than the conventional elastic trial stress, and much less number of iterations was necessary to make convergence in the tests. The plastic trial stress was implemented in ABAQUS/UMAT and 3-dimensional finite element simulation of a tensile test showed that the computation time can be saved by the usage of the plastic trial stress in the material routine without invoking line search strategy.

Only associated flow rule has been assumed and the yield surface was identical to the flow surface in this work. If non-associated flow rule is used, then the flow function will be different to the yield function in general. The concept of the dual plasticity potentials can be applied to non-associated plasticity as well. In that case, the plastic strain rate potential and the flow potential will be in the dual relation as pointed out in [6]. A similar yield potential-based elasto-plastic numerical scheme can be developed in terms of Newton's method, and the concept of the plastic trial stress can be adopted in the non-associated framework. Our future effort will be made on the verification of the numerical efficiency of the plastic trial stress in the non-associated plasticity model.

References

1. Scherzinger WM (2017) A return mapping algorithm for isotropic and anisotropic plasticity models using a line search method. Comput Methods Appl Math 317:526–553
2. Perez-Foguet A, Armero F (2002) On the formulation of closest-point projection algorithms in elastoplasticity-part II: globally convergent schemes. Int J Num Methods Eng 53:331–374

3. Manik T (2021) A natural vector/matrix notation applied in an efficient and robust return-mapping algorithm for advanced yield functions. Euro J Mech A Solids 90. https://doi.org/10.1016/j.euromechsol.2021.104357
4. Ziegler H (1983) An introduction to thermomechanics. North-Holland Pub. Com.
5. Hill R (1950) The mathematical theory of plasticity. Oxford (1950)
6. Yang S, Tong W (2022) Non-quadratic pseudo dual potentials for plastic flow modeling. In: IDDRG 2022 conference. Lorient, France
7. Yang S, Sheng J, Alharbi M, Tong W (2021) On edge crack initiation of an aluminum sheet metal. In: The 13th international conference on the technology of plasticity
8. de Souza Neto EA, Peric D, Owen DRJ (2008) Computational methods for plasticity, theory and applications. Wiley, New York

Anisotropic Time-Dependent Continuum Damage-Coupled Plasticity Model for Predicting Ductile Fracture of 6xxx Series Aluminum Alloys

Mustapha Makki, Georges Ayoub, Andrey Ilinich, and Ghassan Kridli

Abstract An accurate prediction of the fracture strain under different stress states is essential for designing metal formed structures. General stress states may be characterized by two independent parameters; the stress triaxiality ratio and the Lode angle. When both parameters remain constant throughout the strain history, the loading is said to be proportional. In this work, the mechanical and damage behavior of ductile metal was captured using an anisotropic time-dependent continuum damage model coupled plasticity. The model was implemented in a finite element simulation code using an implicit time integration scheme. A hybrid method combining experimental (proportional loading) and finite element simulations was used for the model calibration. The predictive capability of the model with embedded cumulative damage law was validated on proportional loading tests conducted on a 6xxx series aluminum alloy sheets.

Keywords Continuum damage mechanics · Anisotropic damage · Anisotropic plasticity · Proportional loading

Introduction

Stamping operations are used for producing a large number of structural components for the automotive, aerospace, electronics, and telecommunications industries. More specifically, sheet metal forming is of high interest for the automotive industry prompted by the need to produce fuel-efficient vehicles and therefore manufacture intricate shape structural parts at higher rate and lower cost. Furthermore, with the increasing use of lightweight materials for stamping processes new challenges emerged. Aluminum alloys are high specific strength structural metals widely used

M. Makki · G. Ayoub (✉) · G. Kridli
Industrial and Manufacturing Systems Engineering Department, University of Michigan Dearborn, Dearborn, MI 48128, USA
e-mail: gayoub@umich.edu

A. Ilinich
Ford Motor Company, Dearborn, MI 48124, USA

K. Inal et al. (eds.), *NUMISHEET 2022*, The Minerals, Metals & Materials Series,
https://doi.org/10.1007/978-3-031-06212-4_2

by the aerospace and automotive industries. The fracture is an important failure mode limiting the design space feasible for manufacturing and in-service use. Aluminum alloy sheets generally exhibit an anisotropic plastic and fracture behaviors. In this work we propose a novel fracture prediction model that can be used in stamping feasibility assessment.

A considerable number of models were proposed to capture the ductile behavior of metals associated with their mechanical properties degradation. The ductile fracture behavior is characterized by a sequence of degradation mechanisms induced by the plastic deformation, namely; void nucleation, growth, and coalescence [1, 2]. In the literature, we can differentiate among three different types of fracture models. First, the "Gurson type" models explicitly formulate macroscopic yield criterion based on homogenization theories for spherical and cylindrical voids [3–7]. The second type is the phenomenological "uncoupled damage" fracture models formulated without accounting for the damage evolution directly in the elastic and plastic properties [8]. These models make use of damage indicator functions to accumulate damage. The damage increment is proportional to the increment of the effective plastic strain weighted by severity of the stress state. The weighting is a function of two stress state parameters; the stress triaxiality (ratio of the hydrostatic stress to von Mises stress) and Lode angle (third stress invariant) [9–14]. Finally, the "continuum damage mechanics/coupled damage" models are derived from a thermodynamic dissipation potential and account for the damage evolution directly in the elastic and plastic properties [15]. Kachanov first introduced the formulation of the damage variable to predict creep induced fracture in metals [16]. Originally, the effect of damage was quantified using a continuity scalar variable ranging from zero for defect free material to unity for a failed material. Later, the loss of the material's load bearing capability was explained by defining the damage parameter as the ratio between the material's damaged surface and the total surface [17]. Based on that definition, the concept of effective stress linking the damage configuration to a fictitious defect free configuration was proposed [18, 19]. Initially, the continuum damage mechanics model assumed metal to be isotropic [20–22]. After, a multitude of experimental investigations on the ductile fracture of metallic materials reported that the damage is anisotropic, an anisotropic model was developed in which damage is a tensorial variable [23]. The theoretical formulation of the coupled anisotropic damage with plasticity was achieved by replacing the nominal stress with its effective value in the plastic potential function [24].

In this work, the mechanical and damage behavior of a 6xxx aluminum alloy is captured using an anisotropic time-dependent continuum damage-coupled plasticity model. The model was implemented in Abaqus/Standard as a user subroutine, and the parameters were calibrated on the experimental data. A hybrid method combining experimental and FEM simulations was used for the model calibration. The predictive capability of the model with embedded damage cumulative law was validated on proportional loading tests.

Experiments

In this section, the experimental procedure is detailed. Notched tensile specimens with a notch radius of 10 mm (NR10) were tested using a uniaxial tensile testing machine combined with a digital image correlation system (DIC). The material used in this study is a 6xxx aluminum alloy sheet of 1 mm thickness, widely used for stamping outer vehicle body panels. The nominal chemical composition of the studied 6xxx series aluminum alloy is given in Table 1. The material was studied in T4 temper after a substantial amount of natural aging.

An MTS servo-hydraulic machine was used to conduct the experimental tests. The test specimens were machined from a 1 mm Al 6xxx sheet using a wire electrical discharge machine (EDM). The specimens were extracted with their major axis being aligned with either of the rolling direction (RD), diagonal direction (DD), or transverse direction (TD) as shown in Fig. 1.

The test was repeated three times in each direction and the average force vs. displacement is presented in Fig. 1. It was observed that the tested specimens exhibited the same elastic, yield (1.38 kN) and hardening behavior. However, the fracture point was different for the different tested directions. The DD direction exhibited the highest displacement to fracture (2.18 mm).

Table 1 Chemical composition

Element	Si	Mg	Fe	Cu	Mn	Cr	Zn	Ti	Other
Wt%	0.5–1	0.4–0.8	0.3	0.2	0.15	0.1	0.1	0.1	0.15

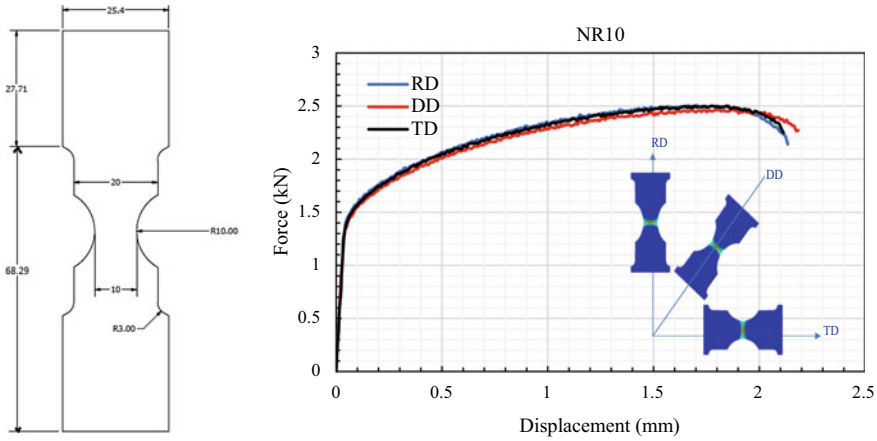

Fig. 1 NR10 specimen geometry and dimensions (in mm), force versus displacement response of specimens extracted from three different material orientations, the inset shows the test specimens' directions: Rolling Direction (RD), Diagonal Direction (DD), and Transversal Direction (TD)

Constitutive Model

In this section, the framework of the anisotropic time-dependent continuum damage-coupled plasticity model is presented. The framework of finite strains was used for developing the model. A detailed description of the model was provided by Kassar et al. [25]. The current work builds upon the previously developed model and proposes the use of damage effect tensor described in the local material coordinate system and not in the principal coordinate system of the damage. We start by providing a brief description of the kinematic variables. The deformation gradient is defined as $\boldsymbol{F} = \nabla \boldsymbol{x}(\boldsymbol{X}, t)$, with $\boldsymbol{x}$ is the coordinates of a material point in the deformed configuration while $\boldsymbol{X}$ is the coordinate of the material point in the undeformed configuration. The deformation gradient can be written as $\boldsymbol{F} = \boldsymbol{F}^e \boldsymbol{F}^p$ with $\boldsymbol{F}^e$ is the elastic part and $\boldsymbol{F}^p$ is the plastic part. The velocity gradient can be written as $\boldsymbol{L} = \dot{\boldsymbol{F}}\boldsymbol{F}^{-1} = \boldsymbol{D} + \boldsymbol{W}$, where $\boldsymbol{W}$ is the spin component (skew-symmetric part) and $\boldsymbol{D}$ is the total rate of deformation (symmetric part). The total rate of deformation can be additively decomposed into elastic and plastic rate for finite deformation $\boldsymbol{D} = \boldsymbol{D}^e + \boldsymbol{D}^p$.

The physical nature of damage induced by the initiation, growth, and coalescence of micro-cracks was quantified by measuring the geometric deterioration of the material's microstructure [26, 27]. For an isotropic case, the damage variable $D = (A - \tilde{A})/A$ is expressed as function of A is the material's total area, and $\tilde{A}$ is the material's total area excluding micro-voids. For the anisotropic case, the effective stress is described as $\tilde{\sigma} = \boldsymbol{M} : \boldsymbol{\sigma}$, where $\boldsymbol{M}(\boldsymbol{D})$ is the fourth-rank linear operator termed damage effect tensor. The damage effect tensor links the damaged material configuration to its fictitious undamaged configuration. For the present investigation, the damage effect tensor was expressed in the local material coordinate system [28]. The elastic energy for a representative volume element under applied stress is expressed as

$$W^e(S) = \frac{1}{2}\sigma_{ij} C^{-1}_{ijkl} \sigma_{kl} \tag{1}$$

where C^{-1}_{ijkl} is the elastic compliance tensor. The elastic energy of the damaged material can be determined by substituting the stress with the effective stress such that $W^e(\boldsymbol{\sigma}, \boldsymbol{D} \neq 0) = W^e(\tilde{\boldsymbol{\sigma}}, \boldsymbol{D} = 0)$. Hence, the expression of the effective elastic compliance tensor is defined as

$$\tilde{C}^{-1}_{ijop} = M_{ijkl} C^{-1}_{klmn} M_{mnop} \tag{2}$$

The visco-plastic constitutive coupled damage equations were developed by replacing the stress tensor with the effective stress tensor in the plastic potential of the undamaged material [29]. Accordingly, the effective Hill equivalent plastic stress is expressed as follows:

$$\tilde{\sigma}_{eq} = \left(\frac{1}{2}\tilde{\sigma} : H : \tilde{\sigma}\right)^{1/2} \tag{3}$$

where the stress $\boldsymbol{\sigma}$ is integrated from the following stress rate expression $\dot{\boldsymbol{\sigma}} = \tilde{\boldsymbol{C}}$ $[\boldsymbol{D} - \boldsymbol{D}^p]$ And $\tilde{C}_{ijop} = M^{-1}_{ijkl} C_{klmn} M^{-1}_{mnop}$, and $\boldsymbol{H}$ is the symmetric fourth-order Hill tensor [30]. The plastic rate of deformation $\boldsymbol{D}^p$ is expressed as follows:

$$D^p_{ij} = \frac{\lambda^p}{2\tilde{S}^{eq}} H_{ijkl} \tilde{S}_{kl} \tag{4}$$

where λ^p is the plastic multiplier approximated by the cumulative plastic strain rate $\dot{p}$ quantified using a visco-plastic strain sensitive power law:

$$\dot{p} = \gamma^p \left(\frac{\tilde{S}^{eq}}{s}\right)^{\frac{1}{m}} \tag{5}$$

where γ^p is the initial plastic rate, m is the strain rate sensitivity parameter and s is the shear strength resistance evolving according to [31].

The damage evolution rate was developed by assuming a dissipative damage potential f^d:

$$\dot{D}^d_{ij} = -\frac{\lambda^d}{2Y^{eq}} L^d_{ijkl} Y_{kl} \tag{6}$$

where λ^d is the Lagrange multiplier term approximated by the cumulative plastic damage rate $\dot{q}$. $\boldsymbol{L}^d$ is a fourth-order plastic damage characteristic tensor. The cumulative plastic damage rate is

$$\lambda^d \approx \dot{q} = \gamma^d \left(\frac{Y^{eq}}{Y^0}\right)^{\frac{1}{n}} \tag{7}$$

where γ^d is the initial damage rate, Y^0 is a damage strengthening resistance, and n is a rate sensitive parameter. The damage strain energy rate is defined as

$$Y_{ij} = -S_{ij} \left\{ C^{-1}_{ijkl} M_{klmn} \frac{\partial M_{mnop}}{\partial D_{qr}} \right\}^s S_{qr} \tag{8}$$

where "s" denotes taking the symmetric part within the curly brackets. Finally, the effective equivalent energy release rate is defined as